Journal of Applied Physics

Thermoelectric properties and stability of $Ba_3Cu_{16-x}Se_{11-y}Te_y$

Cite as: J. Appl. Phys. **126**, 025109 (2019); https://doi.org/10.1063/1.5110043
Submitted: 14 May 2019 . Accepted: 19 June 2019 . Published Online: 11 July 2019

Parisa Jafarzadeh, Abdeljalil Assoud, Daniel Ramirez, Nader Farahi, Tianze Zou, Eckhard Müller, Jan B. Kycia, and Holger Kleinke

Journal of Applied Physics ARTICLE scitation.org/journal/jap

Thermoelectric properties and stability of $Ba_3Cu_{16-x}Se_{11-y}Te_y$

Cite as: J. Appl. Phys. **126**, 025109 (2019); doi: 10.1063/1.5110043
Submitted: 14 May 2019 · Accepted: 19 June 2019 ·
Published Online: 11 July 2019

View Online Export Citation CrossMark

Parisa Jafarzadeh,[1] Abdeljalil Assoud,[1] Daniel Ramirez,[1] Nader Farahi,[2] Tianze Zou,[3] Eckhard Müller,[2,4] Jan B. Kycia,[3] and Holger Kleinke[1,a)]

AFFILIATIONS

[1]Department of Chemistry and Waterloo Institute for Nanotechnology, University of Waterloo, Waterloo, Ontario N2L 3G1, Canada
[2]Institute of Materials Research, German Aerospace Center (DLR), D-51170 Köln, Germany
[3]Department of Physics and Astronomy and Guelph-Waterloo Physics Institute, University of Waterloo, Waterloo, Ontario N2L 3G1, Canada
[4]Institute of Inorganic and Analytical Chemistry, Justus Liebig University Gießen, D-35392 Gießen, Germany

Note: This paper is part of the special topic on Advanced Thermoelectrics.

[a)]**Author to whom correspondence should be addressed:** kleinke@uwaterloo.ca

ABSTRACT

$Ba_3Cu_{16-x}Se_{11-y}Te_y$ materials were synthesized with different compositions by a melting and slow cooling process. Measurement of the thermoelectric properties revealed changes during repeated measurements of the same samples. This scenario is different from the case of the isostructural sulfide variants, where the physical properties were consistently reproducible under the measurement conditions applied. Further investigations including single crystal studies after the measurements proved that this is a consequence of different Cu ion conductivity in selenides and sulfides. The reproducibility of the data was investigated by varying the maximum temperature as well as the current density. The stability of these selenides was highly dependent on the temperature; decreasing the highest measurement temperature led to full reproducibility. Finally, while the selenides exhibited larger electrical conductivity than the sulfides, their figure-of-merit zT only reached a maximum value of 0.49, compared to 0.88 of the sulfides, mostly caused by the smaller Seebeck values of the selenides.

I. INTRODUCTION

Thermoelectric materials generate useful electricity directly from a heat source. The performance of a thermoelectric material is assessed via its dimensionless figure-of-merit, $zT = T\alpha^2\sigma\kappa^{-1}$. In this equation, α, σ, and κ refer to the material's thermopower or Seebeck coefficient, electrical conductivity, and thermal conductivity, respectively. The term $\alpha^2\sigma$ denotes the power factor of the material, which enhances zT when increasing. In contrast, a lower thermal conductivity, $\kappa = \kappa_L + \kappa_e$, with a contribution of the lattice thermal conductivity κ_L and the electronic thermal conductivity κ_e, results in a larger value of zT.[1,2] The interrelation of the electrical conductivity, σ, with the thermal conductivity, κ, causes some difficulties in the enhancement of the zT of the thermoelectric materials. For instance, based on the Wiedemann-Franz law, $\kappa_e = L\sigma T$, a larger σ will cause a higher κ_e. Lastly, in order for a material to be used for thermoelectric applications, both the mechanical and thermal stability need to be outstanding.

Copper chalcogenides, $Cu_{2-x}S$ and β-$Cu_{2-x}Se$, are known for their excellent thermoelectric performances, with zT values of 1.7 and 1.5 at around 1000 K.[3,4] Regardless of their relatively simple crystal structures, these two binaries exhibit a very low κ, $Cu_{1.98}S$ with 0.39 W m^{-1} K^{-1} at 300 K and 0.3 W m^{-1} K^{-1} at 1000 K,[3] and β-Cu_2Se with 1.0 W m^{-1} K^{-1} at 420 K and 0.7 W m^{-1} K^{-1} at 1000 K,[5] due to the liquidlike behavior of the Cu ion sublattice. The concept of phonon-glass electron-crystal (PGEC) was introduced by Slack in the 1990s.[6] PGEC materials usually constitute an electrical conductor (EC) sublattice and another sublattice ideally with the ability of blocking phonons (PG). By reducing the phonon propagation in PGEC materials through reducing the phonon mean free path to the glass limit, these materials are experiencing high zT values, in these cases with $zT > 1$.

β-$Cu_{2-x}Se$ could be considered as a phonon-liquid electron crystal (PLEC). The term PLEC refers to the low heat propagation

by a crystalline material, which can also be regarded to be an extension of PGEC.[5] Unfortunately, the stability of the binary copper chalcogenides, $Cu_{2-x}S$ and β-$Cu_{2-x}Se$, remains an issue. Due to the Cu ion migration throughout the entire material and Cu metal deposition on one side of the device leg as a result, β-$Cu_{2-x}Se$ and Cu_2S show a lack of stability in high temperature thermoelectric devices.[7–9] Ultimately, the reduced Cu concentration inside these materials will impact the resistivity. Adding heteroatoms such as Li,[10] B,[11] and Sn[12] to Cu_2Se as well as adding interfaces with the ability of ion blocking between different segments of a Cu_2Se thermoelectric leg could improve the stability of this material.[7]

Here, incorporating larger elements such as Ba and Te was considered as a strategy to reduce the Cu ion migration. Accordingly, the structures of several quaternary barium copper chalcogenides were uncovered.[13–20] Some of these compounds including isostructural $Ba_3Cu_{16-x}S_{11-y}Te_y$[19] and $Ba_3Cu_{16-x}Se_{11-y}Te_y$[20] only form when mixed occupied chalcogen sites are present. Recently, we proved the high stability of $Ba_3Cu_{16-x}S_{11-y}Te_y$ under the measurement conditions applied.[21] Due to the larger mass fluctuation on the chalcogen sites compared to the other measured samples, $Ba_3Cu_{15.3}S_{7.5}Te_{3.5}$ possessed the lowest lattice thermal conductivity of that series, $\kappa_L < 0.4\ W\ m^{-1}\ K^{-1}$, thereby $zT = 0.88$ was achieved at 745 K.[21] This zT value makes this material comparable with β-Cu_2Se ($zT = 0.82$ at 750 K) and $Cu_{1.98}S$ ($zT = 0.93$ at 750 K).[3,5] With this paper, we are for the first time presenting the full thermoelectric properties as well as the stability investigation of $Ba_3Cu_{16-x}Se_{11-y}Te_y$, after the first article introduced only the crystal structure, electronic structure, and electrical properties (on a cold-pressed bar).[20]

II. EXPERIMENTAL DETAILS

Samples with the nominal composition of $Ba_3Cu_{16-x}Se_{11-y}Te_y$ ($x = 1.3,\ 1.6$; $y = 2.5,\ 2.8,\ 3$) were synthesized from the elements (Ba pieces, 99.7%, Strem Chemicals; Cu powder, 99.5%, Alfa Aesar; Se pellets, 99.9%, Alfa Aesar; Te broken ingots, 99.99%, Strem Chemicals). These values for x and y are well within the phase range ($1 < x < 2$; $2 < y < 4$). Stoichiometric amounts of the elements were loaded into carbon-coated silica tubes in an argon-filled glove box. Thereafter, the tubes were evacuated up to 10^{-3} mbar and sealed using the H_2/O_2 torch. The reactions were carried out in programmable box resistance furnaces, where the tubes were heated up to 1023 K in 12 h. Samples were kept at this temperature for 10 h followed by cooling to 873 K in 20 h and annealing at this temperature for 100 h. Thereafter, the furnace was switched off to allow for fast cooling down to room temperature.

The phase purity of the synthesized compounds was verified by an Inel powder diffractometer, which is equipped with a position-sensitive detector utilizing Cu-$K\alpha_1$ radiation. The X-ray diffraction patterns of the pure phase samples are depicted in Fig. S1.

The ground pure samples were then compacted to round disks with a diameter of 12.7 mm using the hot-press, Oxy-Gon Industries, model FR-210-30T, at 60 MPa at 800 K for 120 min. A density of almost 100% of the theoretical maximal values was achieved. For the physical property measurements, each hot-pressed sample was cut into half, resulting in two cylindrical pellets each with almost 2 g of weight. The thermal diffusivity measurement was performed on one of these pellets, while the other pellet was cut into a rectangular bar to perform the electrical transport property measurements. This ensures that any changes during one measurement would have no impact on the other one.

Thermal diffusivity, λ, was determined on polished hot-pressed pellets using a flash method with the Netzsch LFA 467 under a flow of Argon. Thermal conductivity, κ, was computed via $\kappa = \rho\lambda C_P$. Here, the estimated heat capacity, C_P, was taken from the Dulong-Petit law,[22] with the density ρ being experimentally determined.

The electrical transport properties were performed on rectangular bars of approximate dimensions of $9 \times 2 \times 2\ mm^3$. They were measured with an ULVAC ZEM-3, which utilizes a four-probe electrical conductivity measurement with simultaneous measurement of the Seebeck coefficient, α, above room temperature under helium atmosphere.[23] The experimental errors for the thermal diffusivity, electrical conductivity, and Seebeck measurements are estimated to be ±5%, ±5%, and ±3%, respectively.

Hall measurements were performed on rectangular bars with dimensions of approximately $8 \times 2.5 \times 1$ mm. The sample holder was connected to six leads with pogo pins, and the electrical conductivity was measured using a four-probe AC method utilizing a SRS 830 lock-in amplifier and a PAR190 transformer. The Hall resistance, R_H, was obtained from the measured Hall voltage, V_H, and a known AC current, always below 5 mA, and the outer magnetic field of 0.5 T. From these measurements, the Hall carrier concentration, n, and carrier mobility, μ, were calculated. A Proportional-Integral-Derivative (PID) temperature control system equipped with a Peltier thermoelectric cooler was used to stabilize the temperature. The fairly small statistical error of ±1% related to the error in measuring V_H and the signal voltage, V, is due to the noise of the measurement. The systematic uncertainty of ±3% of the mobility and the carrier density is related to the accuracy of the dimensions of the samples as well as the contact distances.

To check for a possible inhomogeneity after the electrical transport measurements, a Potential-Seebeck-Microprobe (PSM)[24] was utilized on a bar of nominal composition $Ba_3Cu_{14.7}Se_{8.2}Te_{2.8}$ with dimensions of $10 \times 2 \times 1.6\ mm^3$ at room temperature. The PSM provides a two-dimensional image of the Seebeck values of the whole sample by moving the probe tip from point to point across the surface.

The room temperature X-ray single crystal analyses were performed on a single crystal of $Ba_3Cu_{14.7}Se_{8.5}Te_{2.5}$ before hot-pressing and after the electrical transport property measurements. The single crystals were selected under an optical microscope with all edges <70 μm after crushing the polycrystalline samples. A Bruker Kappa Apex II CCD that employs Mo-Kα radiation was utilized for the data collection on black blocklike crystals. Using the search strategy of the APEX II suite, ω scans were performed in different sets of frames for full data coverage. The exposure time was 30 s/frame. The collected data were treated for Lorentz and polarization effect corrections. Absorption corrections were done based on the empirical multiscan method SADABS as a part of the APEX II package.[25]

The refinement[26] of a crystal from the sample of the nominal composition $Ba_3Cu_{14.7}Se_{8.5}Te_{2.5}$ before hot-pressing the sample with six Cu atom sites using the published model of $Ba_3Cu_{16-x}Se_{11-y}Te_y$[20] in the space group $R\bar{3}m$ resulted in $R(F_o) = 0.071$. Large electron densities remained, namely, 10.8 e Å^{-3}, 8.5 e Å^{-3}, and 4.5 e Å^{-3},

respectively. The positions of these three high residual electron densities were all surrounded by four chalcogen atoms at the appropriate Cu–Se/Te distances. Including these three positions as additional Cu7, Cu8, and Cu9 positions decreased the highest peaks in the difference Fourier map to acceptable values <3 e Å^{-3}, which lowered $R(F_o)$ to 0.047. Their refined occupancies were 0.26(1), 0.21(1), and 0.067(8), respectively. The formula was thus refined to be $Ba_3Cu_{14.59(8)}Se_{8.96(5)}Te_{2.04}$.

The refinement of a single crystal of the same sample after the electrical transport property measurements with the initial six Cu atom sites resulted in even larger residual electron densities of 25.9 e Å^{-3}, 24.7 e Å^{-3}, and 24.3 e Å^{-3}, and an unacceptable $R(F_o) = 0.148$. Again refining these as Cu-deficient sites yielded a final value of $R(F_o) = 0.033$, with larger occupancies of 0.448(7), 0.339(7), and 0.309(4) for Cu7, Cu8, and Cu9, respectively, compared to the crystal before the property measurement and the largest remaining electron density being 4.6 e Å^{-3}. The obtained formula of $Ba_3Cu_{14.60(2)}Se_{8.97(5)}Te_{2.03}$ is equal within one standard deviation to the one from before the property measurements, while the distribution of the Cu atoms changed significantly, with Cu2–Cu5 showing smaller occupancies and Cu7–Cu9 showing larger occupancies. The different distribution implies an irreversible movement of the Cu atoms either under the electric field or the temperature gradient applied during the measurements. Tables S1 and S2 contain the crystallographic details, fractional atomic coordinates, equivalent isotropic displacement parameters, and site occupancies for these two data sets.

In contrast to the selenides with different occupations of nine Cu sites, a single crystal structure refinement of a crystal of the nominal composition $Ba_3Cu_{15.1}S_{8.5}Te_{2.5}$ after the electrical property measurements with six Cu sites resulted in a maximum residual electron density of 4.3 e Å^{-3} and a good value of $R(F_o) = 0.038$ with no additional Cu sites.

The Cu contents after the last measurements of the electrical transport properties were investigated through SEM/EDX (Scanning Electron Microscopy/Energy-Dispersive X-ray analysis). The measurements were performed on the top and bottom of the measured bars. The QuantaFeg 250/Oxford instrument x-act with the applied acceleration voltage of 20 kV was used for this purpose.

III. RESULTS AND DISCUSSION

The crystal structure of $Ba_3Cu_{16-x}Se_{11-y}Te_y$ is isostructural with the rhombohedral variant of $Ba_3Cu_{16-x}S_{11-y}Te_y$. This structure is composed of CuQ_4 tetrahedral units [with shared chalcogen atom sites (Q = Se/Te)] that construct a three-dimensional network via corner-, face-, and edge-sharing (Fig. 1). Of the five crystallographically independent Q sites, two are always Se sites, one a Te site, one a mixed Se/Te site, and one an Se with up to 10% Te. The one Ba site is surrounded by eight Q atoms in the form of a bicapped trigonal prism.

In this structure, the formally d^{10}–d^{10} closed-shell interactions between the Cu atoms occur due to the hybridization of the filled *d* orbitals with the empty *s* and *p* orbitals.[27,28] The occurrence of such bonds in coinage chalcogenides is not rare; other examples include $BaCu_{6-x}Se_{6-y}Te_y$,[17] $Ba_3Cu_{14-x}Te_{12}$,[13] $Tl_2Ag_{12}Se_7$,[29] and $Tl_2Ag_{12}Te_7$.[30] These Cu–Cu bonds, all shorter

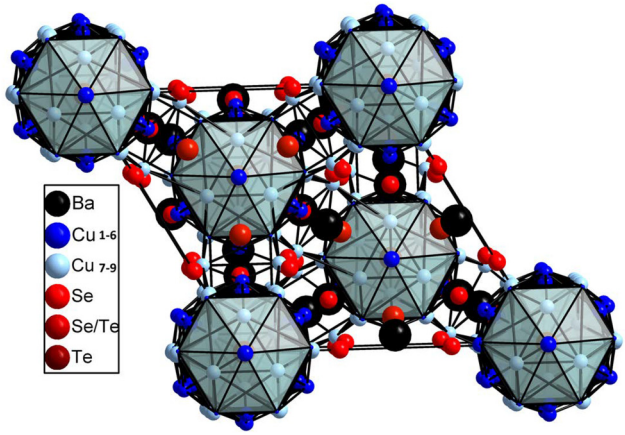

FIG. 1. Crystal structure of $Ba_3Cu_{16-x}Se_{11-y}Te_y$ in a projection onto the *a*, *b* plane. The Cu atom clusters are highlighted as polyhedra.

than 3 Å, not only result in the formation of Cu clusters with 26 Cu atoms but also bond these clusters in three dimensions. As a consequence of the Cu-deficient sites combined with the three-dimensional clusters, about 7% of the Cu ions could be successfully replaced at room temperature with Ag atoms, indicative of substantial Cu atom mobility.[20]

Both structures, $Ba_3Cu_{16-x}S_{11-y}Te_y$ and $Ba_3Cu_{16-x}Se_{11-y}Te_y$, are composed of the three-dimensional Cu clusters and the Cu-deficient sites. However, more Cu sites are occupied in the selenides, resulting in a larger disorder (Fig. 2), as evident from single crystal structure studies. The occupancy of these sites denoted as Cu7, Cu8, and Cu9, are 26%, 21%, and 7% before the electrical transport property measurements and 45%, 34%, and 31% after the measurements, respectively.

According to previous density functional theory (DFT) calculations,[20] the electron-precise material with exactly 16 Cu atoms per formula unit, $(Ba^{2+})_3(Cu^+)_{16}(Q^{2-})_{11}$, behaves as a semiconductor. The calculated bandgap of 0.02 eV along with the Cu atom deficiency results in a heavily doped *p*-type semiconductor.

The temperature dependent electrical conductivity, σ, of the measured samples ($x = 1.3$, 1.6 and $y = 2.5$, 3) upon heating and cooling is shown in Fig. 3. As can be seen in all heating measurement plots, σ initially decreases with increasing temperature. This behavior is typical for extrinsic semiconductors, caused by the decrease in the electron mobility, μ, with increasing temperature, while the (extrinsic) carrier concentration remains largely unchanged. σ then begins to increase around 580 K–600 K, potentially because of the change in the occupancies of the Cu atom sites. With the estimated relative error of ±5%, samples with the same amount of *y* exhibit the same σ within the measured temperature range. On the other hand, as was also seen previously for the sulfides, materials with larger Te content exhibit larger σ. This can be explained by the different covalent character; the higher covalency of the Ba–Te and Cu–Te bonds as compared to Ba–Se and Cu–Se occurs with a higher carrier mobility for the materials with higher Te concentration.

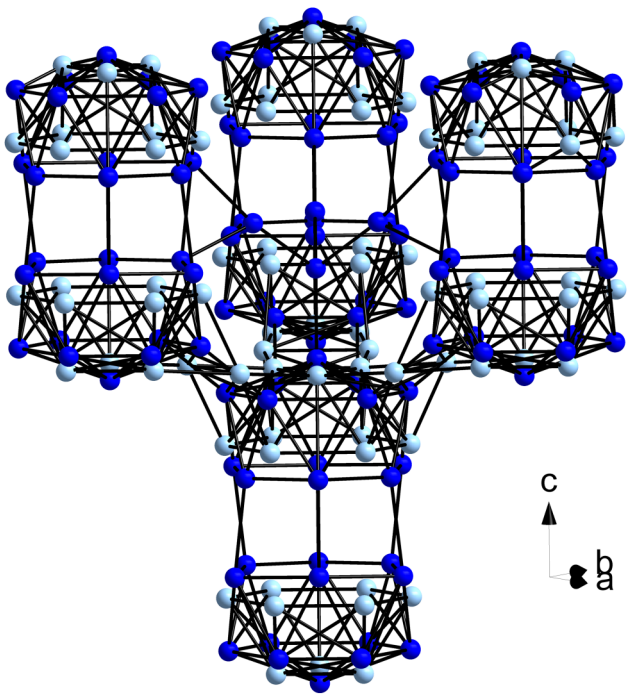

FIG. 2. Three-dimensional network of Cu clusters in the structure of $Ba_3Cu_{16-x}Se_{11-y}Te_y$. Cu7, Cu8, and Cu9 are in bright blue and the other Cu sites in dark blue.

Correspondingly, the σ values for the samples with $x = 1.6$ and $y = 3$ (i.e., 3 Te per formula unit) range from 385 Ω^{-1} cm^{-1} at 299 K to 280 Ω^{-1} cm^{-1} at 695 K, while the ones with $y = 2.5$ vary from 338 Ω^{-1} cm^{-1} to 264 Ω^{-1} cm^{-1}.

In contrast to the sulfide variants, the measurements result in different values when repeated. In all the measured cases, cooling (open symbols) yields larger values of σ compared to heating (closed symbols). A larger mismatch between the heating and cooling data up to ~40% can be observed at lower temperatures. The measured electrical conductivity of the cooling process constantly increases with decreasing temperature with a maximum of 466 Ω^{-1} cm^{-1} for $Ba_3Cu_{14.4}Se_{8.5}Te_{2.5}$ at 300 K and a minimum of 242 Ω^{-1} cm^{-1} for $Ba_3Cu_{14.7}Se_{8.5}Te_{2.5}$ at 695 K. The larger electrical conductivity of the cooling measurement compared to the same temperatures during heating is likely a consequence of Cu ion movement causing irreversible changes in this material, as also observed in the cases of Cu_2S and Cu_2Se.

To investigate whether the electrical conductivity would continue to change from measurement to measurement, we repeated these electrical transport measurements twice in the case of $Ba_3Cu_{14.7}Se_{8.5}Te_{2.5}$. The values did not change noticeably after the first measurement (Fig. S2), indicating that a steady state was reached, and the materials remain stable after one measurement. However, in some cases, the steady state was reached later, e.g., after three or four cycles, or not at all during the first four cycles, as demonstrated for the slightly more Te-rich $Ba_3Cu_{14.7}Se_{8.2}Te_{2.8}$ (Fig. S3).

In order to investigate whether this is an annealing effect, a hot-pressed bar of a sample of nominal composition $Ba_3Cu_{14.4}Se_{8.5}Te_{2.5}$ was annealed for 3 weeks prior to any physical property measurements at 700 K. Similar to the data before annealing, the electrical transport properties after 3 weeks of annealing revealed a lack of stability after the first heating measurement (Fig. S4). The electrical conductivity at 300 K was measured to be 334 Ω^{-1} cm^{-1} at the beginning and 384 Ω^{-1} cm^{-1} at the end of the first measurement cycle, corresponding to an increase of 15%. This implies that the larger electrical conductivity after the first heating is not simply a consequence of an annealing effect, but caused by the measurement conditions, i.e., either by the voltage or the temperature gradient.

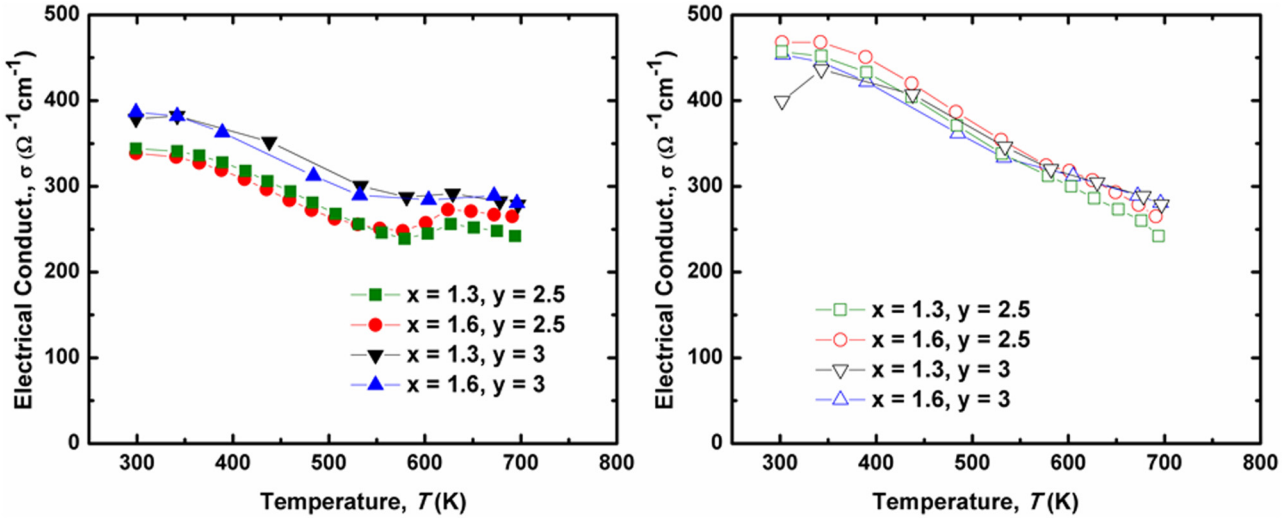

FIG. 3. Electrical conductivity of the heating (left) and cooling (right) measurements of $Ba_3Cu_{16-x}Se_{11-y}Te_y$ in dependence on the temperature.

To investigate the cause for the variation of the σ values during these measurements, room temperature Hall measurements were done on the samples of $Ba_3Cu_{14.4}Se_{8.5}Te_{2.5}$ and $Ba_3Cu_{14.4}Se_8Te_3$. In each case, two different bars from the same hot-pressed pellet were measured. The Hall measurement on the first bar was done directly after hot-pressing, while the second bar was measured after the electrical transport property measurements. The positive R_H in all cases is indicative of the *p*-type semiconducting behavior of these materials with holes as dominant charge carriers. The electrical conductivity values increased from 325 Ω^{-1} cm^{-1} to 456 Ω^{-1} cm^{-1} for $Ba_3Cu_{14.4}Se_{8.5}Te_{2.5}$ and from 370 Ω^{-1} cm^{-1} to 449 Ω^{-1} cm^{-1} for $Ba_3Cu_{14.4}Se_8Te_3$, i.e., by 40% and 21%, respectively, comparing the data from before and after the property measurements. This compares well with the data from the ZEM apparatus: there, the room temperature electrical conductivity of these samples increased from 338 Ω^{-1} cm^{-1} to 466 Ω^{-1} cm^{-1} for $Ba_3Cu_{14.4}Se_{8.5}Te_{2.5}$ and from 385 Ω^{-1} cm^{-1} to 451 Ω^{-1} cm^{-1} for $Ba_3Cu_{14.4}Se_8Te_3$ at the beginning vs the end of the first measurement cycle (i.e., by 38% and 17%).

The charge carrier concentrations increased also, namely, from 3.3×10^{20} cm^{-3} to 4.0×10^{20} cm^{-3} for $Ba_3Cu_{14.4}Se_{8.5}Te_{2.5}$, and from 3.2×10^{20} cm^{-3} to 4.7×10^{20} cm^{-3} for $Ba_3Cu_{14.4}Se_8Te_3$. On the other hand, the carrier mobility changed differently in the two samples, with one increasing from 6.4 cm^2 V^{-1} s^{-1} to 7.3 cm^2 V^{-1} s^{-1} ($Ba_3Cu_{14.4}Se_{8.5}Te_{2.5}$), and the other decreasing from 7.5 cm^2 V^{-1} s^{-1} to 6.0 cm^2 V^{-1} s^{-1} ($Ba_3Cu_{14.4}Se_8Te_3$). The latter may be a consequence of the more significantly increased carrier concentration resulting in enhanced carrier-carrier scattering.

The temperature dependences of the Seebeck coefficient, α, of the measured samples are depicted in Fig. 4. The general increase of the positive Seebeck coefficient values through the entire temperature range is indicative of heavily doped *p*-type semiconductors. As in the case of the electrical conductivity, the cooling data differ from the heating data. For instance, the α values for the first heating measurement of $Ba_3Cu_{14.7}Se_{8.5}Te_{2.5}$ range from 65 μV K^{-1} at 300 K to 136 μV K^{-1} at 695 K, while the α value measured during cooling is 55 μV K^{-1} at 300 K, corresponding to a decrease of 18%. It is noted that these changes generally appear to be relatively smaller than in the case of the electrical conductivity. The heating and cooling measurements repeated for two more times revealed no more noticeable changes, as was also observed in the case of the electrical conductivity (Fig. S2).

In order to investigate the stability range of $Ba_3Cu_{16-x}Se_{11-y}Te_y$, different current densities and maximum temperatures were applied during the electrical transport measurements. For this purpose, a 4 g sample of $Ba_3Cu_{14.7}Se_{8.5}Te_{2.5}$ was prepared, consolidated into a pellet, then cut into several bars. During the measurements, the current flow alternated direction; however, using a fixed current flow from bottom to top resulted in qualitatively equivalent data. During the Seebeck measurement, the applied temperature gradient always went from bottom to top, with a maximum $\Delta T = 4$ K. As a starting point, the same conditions as for the data shown in Fig. 3 were applied. Those corresponded to a current density equal to the one for the sulfide measurements, namely, 0.084 A cm^{-2}. As expected, the data clearly show a lack of stability in analogy to Fig. 3. With the same maximum temperature but a lower current density of $J = 0.024$ A cm^{-2} at room temperature, a similar lack of stability was still observed. Lowering the maximum temperature to 630 K with the same current density of 0.024 A cm^{-2} still did not readily result in reproducible data, not even with a lower current density of 0.005 A cm^{-2}. When decreasing the maximum temperature to 580 K and using that low current density, reproducible data were finally obtained (Fig. 5), likely because the Cu atom mobility is significantly less at 580 K than at 630 K, let alone at 690 K. This is a consequence of the thermal activation of the Cu atom mobility. We note that 580 K is the temperature where the first irregularities occurred during the electrical conductivity measurements described above. The different applied conditions for evaluating the stability of these materials are listed in Table I.

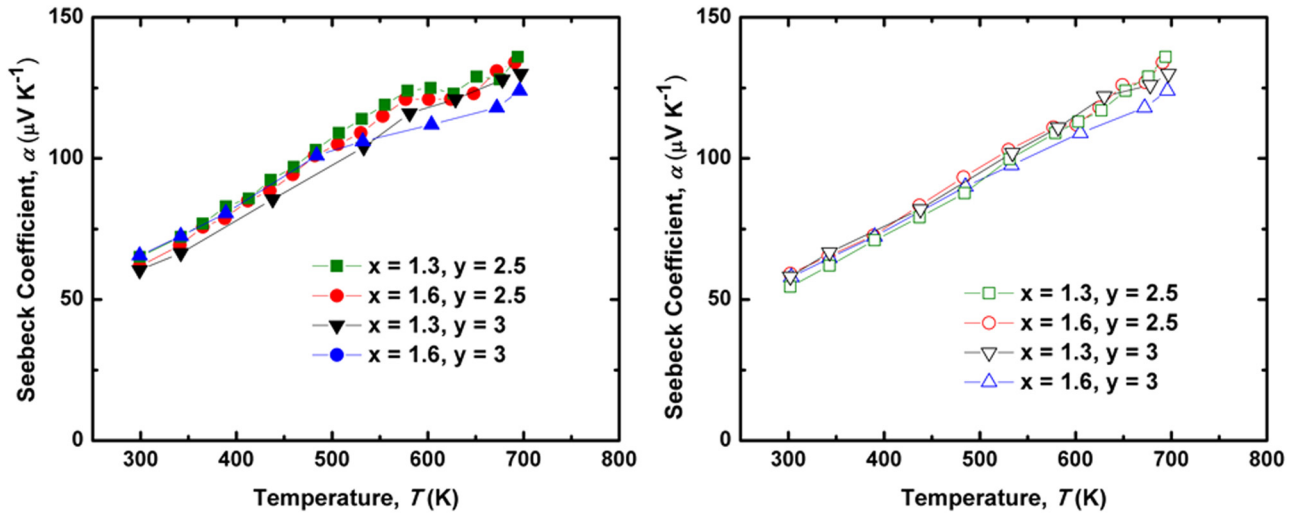

FIG. 4. Seebeck coefficient of the heating (left) and cooling (right) measurements of $Ba_3Cu_{16-x}Se_{11-y}Te_y$ in dependence on the temperature.

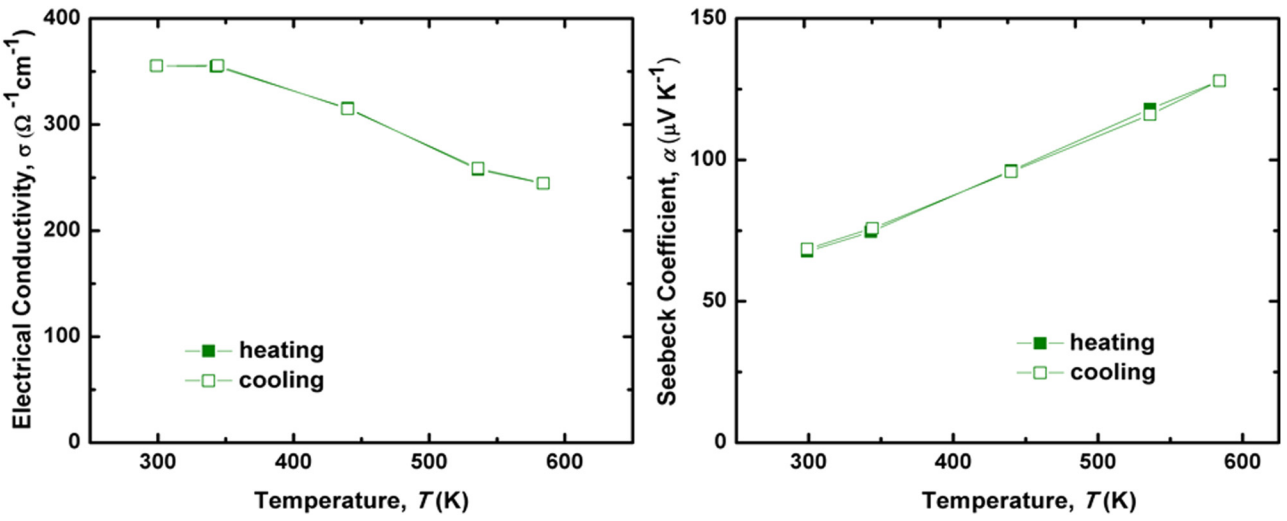

FIG. 5. Stability of the electrical transport properties of $Ba_3Cu_{14.7}Se_{8.5}Te_{2.5}$.

In order to see whether an irreversible Cu ion movement occurred during the measurements, the elemental atomic percentage of Cu after three measurements of a bar of nominal composition $Ba_3Cu_{14.7}Se_{8.5}Te_{2.5}$ with a maximum measured temperature of 690 K, and $J = 0.084$ A cm^{-2} was determined at two different locations via SEM/EDX measurements. The bottom of the bar, which was closer to the heater, showed 44 at. % for copper, while the top of the bar had 50 at.% of copper. This gradient implies an in part irreproducible movement of Cu ions from the bottom to the top of the bar, which corresponds to a movement from the hot side to the cold side during the Seebeck measurement (while the current direction alternated). Additionally, we performed a PSM measurement on a bar of nominal composition $Ba_3Cu_{14.7}Se_{8.2}Te_{2.8}$, using a $\Delta T = 5$ K at room temperature, which underwent an electrical transport property measurement using the HT-S-σ setup at DLR.[31] This measurement also revealed inhomogeneities in accordance with the changes in the Cu concentration (Fig. 6).

The thermal conductivity, κ, data of the measured samples for both heating and cooling process are depicted in Fig. 7. In both cases, the thermal conductivity values of all samples are rather low ($\kappa < 0.8$ W m^{-1} K^{-1}). κ shows an increase at lower temperatures of the cooling measurement compared to that temperature in the heating process. For example, in $Ba_3Cu_{14.7}Se_{8.5}Te_{2.5}$, the room temperature value of the first heating measurement is 0.64 W m^{-1} K^{-1} and 0.69 W m^{-1} K^{-1} after cooling, corresponding to a relatively small increase of 8%, compared to the changes in the electrical properties. A lack of stability—albeit with a smaller change—is thus also observed during the thermal diffusivity measurements, as a noticeable temperature gradient is also applied in the flash method. As in the case of the electrical data, repeated cycling leads sooner or later to reproducible values (Fig. S5).

Samples with the larger amount of Te atoms exhibit lower κ, with the same values within the experimental error for

TABLE I. Different applied conditions to investigate the stability of $Ba_3Cu_{14.7}Se_{8.5}Te_{2.5}$ compared to $Ba_3Cu_{15.1}S_{8.5}Te_{2.5}$.

Chemical formula	T_{max} (K)	J (A cm^{-2})
$Ba_3Cu_{15.1}S_{8.5}Te_{2.5}$	690	0.084
$Ba_3Cu_{14.7}Se_{8.5}Te_{2.5}$	690	0.084
$Ba_3Cu_{14.7}Se_{8.5}Te_{2.5}$	690	0.024
$Ba_3Cu_{14.7}Se_{8.5}Te_{2.5}$	630	0.024
$Ba_3Cu_{14.7}Se_{8.5}Te_{2.5}$	630	0.005
$Ba_3Cu_{14.7}Se_{8.5}Te_{2.5}$	580	0.005

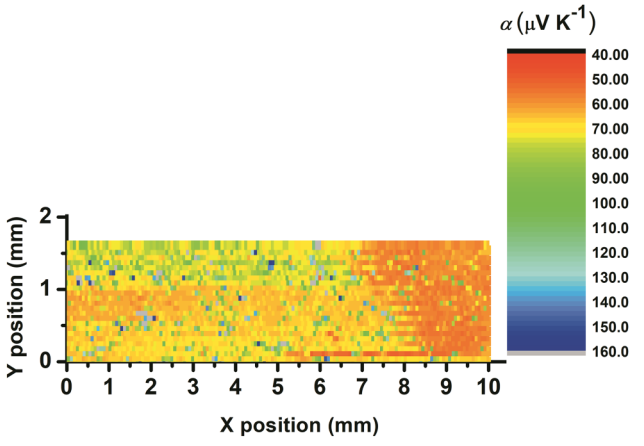

FIG. 6. Spatial resolution of the Seebeck coefficient of $Ba_3Cu_{14.7}Se_{8.2}Te_{2.8}$.

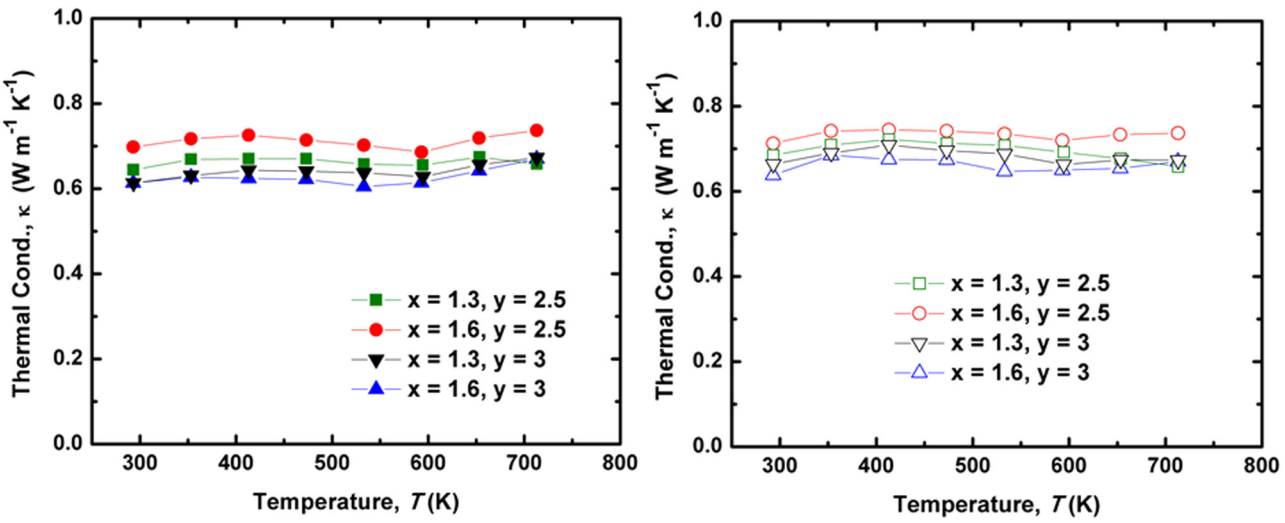

FIG. 7. Thermal conductivity of the heating (left) and cooling (right) measurements of $Ba_3Cu_{16-x}Se_{11-y}Te_y$ in dependence on the temperature.

$Ba_3Cu_{14.4}Se_8Te_3$ and $Ba_3Cu_{14.7}Se_8Te_3$, with $\kappa = 0.61$ W m^{-1} K^{-1} at the beginning of the data collection. This observation is in correlation with the larger mass fluctuation for the samples with the larger Te concentration.

These thermal conductivity values are larger than the values of $Ba_3Cu_{16-x}S_{11-y}Te_y$. Specifically, the low temperature thermal conductivity value for $Ba_3Cu_{15.1}S_{8.5}Te_{2.5}$, 0.53 W m^{-1} K^{-1}, which has the largest thermal conductivity among the three measured sulfides, is lower than the lowest thermal conductivity of the measured selenides.

In any case, the lower thermal conductivity of these materials is comparable with some of the well-known materials with low lattice thermal conductivity at elevated temperatures up to 800 K. In $Ag_nPb_mM_nTe_{m+2n}$ (M = Sb or Bi) and more specifically $AgPb_{10}SbTe_{12}$ ($\kappa_L \sim 1$ W m^{-1} K^{-1} at 650 K),[32] phonon scattering through the grain boundaries reduces the lattice thermal conductivity, and thereby the thermal conductivity decreases. On the other hand, the low thermal conductivity of the filled skutterudites is a consequence of the incorporated rattling atoms inside the large voids,[33] while some materials such as β-Zn_4Sb_3 and Ag_2Te decrease the thermal conductivity due to the presence of the large deficiencies in some of the cation sites.[34–36]

As discussed in Sec. I, the thermal conductivity, κ, is a sum of the electronic thermal conductivity, κ_e, and the lattice thermal conductivity, κ_L. To gain further insight into the effect of the mass fluctuation on the lattice thermal conductivity, κ_L, via $\kappa_L = \kappa - \kappa_e$ was calculated. Here, κ_e was estimated from the Wiedemann-Franz law, $\kappa_e = L\sigma T$. The Lorenz number L was computed by applying the proposed Eq. (1) under the assumption of acoustic phonons, which was reported to be in good agreement with the single parabolic band (SPB) model.[37] We refrained from calculating κ_e from the cooling data, as the electrical conductivity changed more significantly than the thermal data. Therefore, only the heating data can be provided for the lattice thermal conductivity (Fig. 8),

$$L = \left(1.5 + \exp\left[\frac{-|\alpha|}{116\ \mu\text{V/K}}\right]\right) 10^{-8}\ \text{V}^2\ \text{K}^{-2}. \quad (1)$$

Consistently, all samples possess very low κ_L values, namely, below 0.6 W m^{-1} K^{-1}. Samples with the larger mass fluctuation showed similar values to each other and lower values than the other measured samples (e.g., 0.38 W m^{-1} K^{-1} at 299 K and 0.31 W m^{-1} K^{-1}

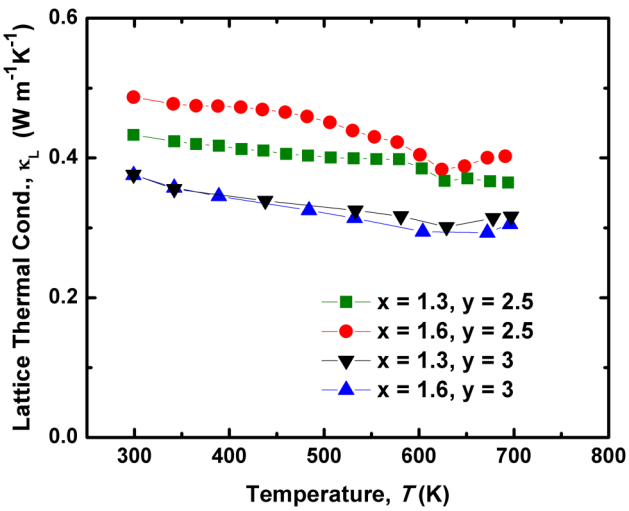

FIG. 8. Lattice thermal conductivity of the heating measurements of $Ba_3Cu_{16-x}Se_{11-y}Te_y$ in dependence on the temperature.

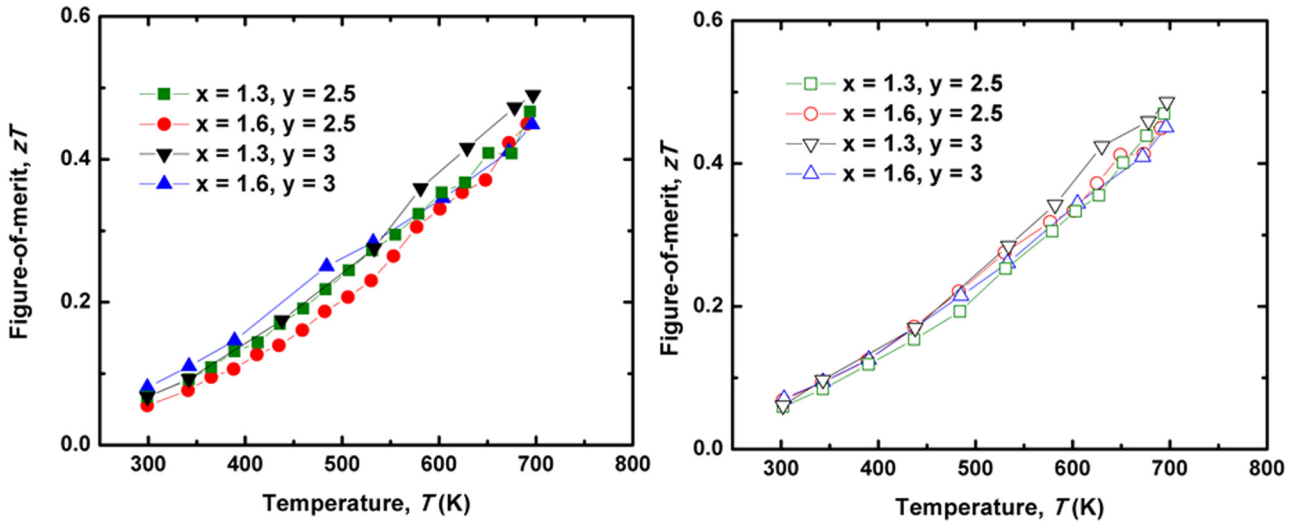

FIG. 9. Thermoelectric figure-of-merit zT of the heating (left) and cooling (right) measurements of $Ba_3Cu_{16-x}Se_{11-y}Te_y$ in dependence on the temperature.

for $x = 1.6$ and $y = 3$). Since κ_L is calculated from $\kappa_L = \kappa - \kappa_e$, i.e., from two determined properties with errors of 5% or higher, the almost 10% difference between the calculated lattice thermal conductivity of $Ba_3Cu_{14.4}Se_{8.5}Te_{2.5}$ and $Ba_3Cu_{14.7}Se_{8.5}Te_{2.5}$ is at the border of significance.

Ultimately, the figure-of-merit was obtained from the fit of the power factor, $\alpha^2\sigma$, with the thermal conductivity values. It should be noted that a zT calculation here has an additional error arising from the different changes in the electrical properties, compared to the thermal ones. An overall increase in the zT curves was observed in the entire measured temperature range for both heating and cooling measured values, caused by generally decreasing the electrical conductivity and by increasing the Seebeck coefficient with the temperature, and a mostly temperature independent thermal conductivity. The maximum computed zT value is obtained for $Ba_3Cu_{14.7}Se_8Te_3$ with $zT = 0.49$ at 695 K, while the other samples' zT_{max} values are equivalent within the error (Fig. 9). Overall, the zT values are smaller than those for the sulfides. For instance, the to date best sulfide sample, $Ba_3Cu_{15.3}S_{7.5}Te_{3.5}$, exhibits zT values of 0.75 around 695 K and 0.88 at 745 K.

IV. CONCLUSION

Polycrystalline copper chalcogenides, $Ba_3Cu_{16-x}Se_{11-y}Te_y$ ($x = 1.3$, 1.6 and $y = 2.5$, 2.8, and 3), have been synthesized. The physical properties of the hot-pressed samples with relative densities of almost 100% of the theoretical maximal values were determined. A lack of stability of the transport properties when measured up to 630 K or higher was observed. Limiting the measurements of the electrical transport properties up to 580 K revealed a good stability of these materials, while in the isostructural sulfides, stable measurements were performed up to 745 K. This is a consequence of a lower Cu ion mobility in the sulfides, most likely arising from the lower polarizability of the harder S anions, compared to Se.

In comparison to $Ba_3Cu_{16-x}S_{11-y}Te_y$, the presence of more occupied Cu sites in the structure of $Ba_3Cu_{16-x}Se_{11-y}Te_y$ resulted in more disorder. Based on room temperature X-ray single crystal data, the distribution of the Cu atoms across the nine Cu sites changed during the electrical property measurements, which is indicative of an irreversible Cu ion movement during these measurements. The irreversible Cu ion movement was verified after the electrical property measurements through SEM/EDX measurements. The 6% difference between the atomic percentage of copper of the bottom and top of the measured bar corresponds to a movement of Cu ions from the hot end to the cold end due to the temperature gradient during the Seebeck measurement. As a result of the irreversible Cu ion movement in these materials, the electrical conductivity and the Seebeck coefficient of the first cooling measurement compared to the same temperature during the first heating exhibited larger and smaller values, respectively, and in some cases later, a steady state was reached, meaning that the electrical properties remained unchanged during subsequent measurements. Similarly, a lack of stability was observed during the thermal diffusivity measurements, as a noticeable temperature gradient was also applied in the flash method.

Finally, the calculated dimensionless thermoelectric figure-of-merit values range from $zT = 0.44$ to $zT = 0.49$ for all the measured samples around 690 K. These zT values are not comparable with those of the sulfide variants, which culminated in 0.75 around 695 K and 0.88 at 745 K for $Ba_3Cu_{15.3}Se_{7.5}Te_{3.5}$. In conclusion, the sulfides are preferred over the selenides for thermoelectric applications because of their higher stability and better performance (and lower toxicity).

SUPPLEMENTARY MATERIAL

See the supplementary material for five figures detailing powder diffraction patterns, repeated measurements of the physical

properties, and results after long time annealing, and two tables listing single crystal data.

ACKNOWLEDGMENTS

We gratefully acknowledge the financial support from the Natural Sciences and Engineering Research Council of Canada in the form of a Discovery Grant (No. RGPIN-2015-04584). We would like to appreciate the endorsement from the DLR Executive Board Member for Space Research and Technology and the support from the Young Research Group Leader Program. We would also like to thank P. Blaschkewitz from DLR for his support with the thermoelectric measurements.

REFERENCES

[1]F. J. DiSalvo, Science **285**, 703 (1999).
[2]Y. Shi, C. Sturm, and H. Kleinke, J. Solid State Chem. **270**, 273 (2019).
[3]Y. He, T. Day, T. Zhang, H. Liu, X. Shi, L. Chen, and G. J. Snyder, Adv. Mater. **26**, 3974 (2014).
[4]B. Yu, W. Liu, S. Chen, H. Wang, H. Wang, G. Chen, and Z. Ren, Nano Energy **1**, 472 (2012).
[5]H. Liu, X. Shi, F. Xu, L. Zhang, W. Zhang, L. Chen, Q. Li, C. Uher, T. Day, and G. J. Snyder, Nat. Mater. **11**, 422 (2012).
[6]G. A. Slack, in *CRC Handbook of Thermoelectrics*, edited by D. M. Rowe (CRC Press, Boca Raton, FL, 1995), pp. 407–440.
[7]P. Qiu, M. T. Agne, Y. Liu, Y. Zhu, H. Chen, T. Mao, J. Yang, W. Zhang, S. M. Haile, W. G. Zeier, J. Janek, C. Uher, X. Shi, L. Chen, and G. J. Snyder, Nat. Commun. **9**, 4 (2018).
[8]D. R. Brown, T. Day, T. Caillat, and G. J. Snyder, J. Electron. Mater. **42**, 2014 (2013).
[9]L. Zhao, X. Wang, F. Y. Fei, J. Wang, Z. Cheng, S. Dou, J. Wang, and G. J. Snyder, J. Mater. Chem. A **3**, 9432 (2015).
[10]S. D. Kang, J.-H. Pöhls, U. Aydemir, P. Qiu, C. C. Stoumpos, R. Hanus, M. A. White, X. Shi, L. Chen, M. G. Kanatzidis, and G. J. Snyder, Mater. Today Phys. **1**, 7 (2017).
[11]S. M. K. N. Islam, M. Li, U. Aydemir, X. Shi, L. Chen, G.J. Snyder, and X. Wang, J. Mater. Chem. A **6**, 18409 (2018).
[12]T. P. Bailey, S. Hui, H. Xie, A. Olvera, and P. F. P. Poudeu, J. Mater. Chem. A **4**, 17225 (2016).
[13]A. Assoud, S. Thomas, B. Sutherland, H. Zhang, T. M. Tritt, and H. Kleinke, Chem. Mater. **18**, 3866 (2006).
[14]Y. Cui, A. Assoud, J. Xu, and H. Kleinke, Inorg. Chem. **46**, 1215 (2007).
[15]O. Mayasree, Y. Cui, A. Assoud, and H. Kleinke, Inorg. Chem. **49**, 6518 (2010).
[16]O. Mayasree, C. R. Sankar, A. Assoud, and H. Kleinke, Inorg. Chem. **50**, 4580 (2011).
[17]O. Mayasree, C. R. Sankar, Y. Cui, A. Assoud, and H. Kleinke, Eur. J. Inorg. Chem. **2011**, 4037 (2011).
[18]A. Assoud, J. Xu, and H. Kleinke, Inorg. Chem. **46**, 9906 (2007).
[19]B. A. Kuropatwa, A. Assoud, and H. Kleinke, Inorg. Chem. **50**, 7831 (2011).
[20]B. Kuropatwa, Y. Cui, A. Assoud, and H. Kleinke, Chem. Mater. **21**, 88 (2009).
[21]P. Jafarzadeh, M. Oudah, A. Assoud, N. Farahi, E. Müller, and H. Kleinke, J. Mater. Chem. C **6**, 13043 (2018).
[22]H. Wang, W. D. Porter, H. Böttner, J. König, L. Chen, S. Bai, T. M. Tritt, A. Mayolett, J. Senawiratne, C. Smith, F. Harris, P. Gilbert, J. W. Sharp, J. Lo, H. Kleinke, and L. I. Kiss, J. Electron. Mater. **42**, 1073 (2013).
[23]H. Wang, W. D. Porter, H. Böttner, J. König, L. Chen, S. Bai, T. M. Tritt, A. Mayolet, J. Senawiratne, C. Smith, F. Harris, P. Gilbert, J. W. Sharp, J. Lo, H. Kleinke, and L. Kiss, J. Electron. Mater. **42**, 654 (2013).
[24]D. Platzek, G. Karpinski, C. Stiewe, P. Ziolkowski, C. Drasar, and E. Müller, in *24th International Conference on Thermoelectrics*, *ICT 2005* (IEEE, 2005), pp. 13–16.
[25]*M86-Exx078 APEX2 User Manual* (Bruker AXS Inc., Madison, WI, 2006).
[26]G. M. Sheldrick, Acta Crystallogr. A **64**, 112 (2008).
[27]K. M. Merz, Jr. and R. Hoffmann, Inorg. Chem. **27**, 2120 (1988).
[28]P. K. Mehrotra and R. Hoffmann, Inorg. Chem. **17**, 2187 (1978).
[29]Y. Shi, A. Assoud, C. R. Sankar, and H. Kleinke, Chem. Mater. **29**, 9565 (2017).
[30]Y. Shi, A. Assoud, S. Ponou, S. Lidin, and H. Kleinke, J. Am. Chem. Soc. **140**, 8578 (2018).
[31]J. de Boor, C. Stiewe, P. Ziolkowski, T. Dasgupta, G. Karpinski, E. Lenz, F. Edler, and E. Müller, J. Electron. Mater. **42**, 1711 (2013).
[32]K. F. Hsu, S. Loo, F. Guo, W. Chen, J. S. Dyck, C. Uher, T. Hogan, E. K. Polychroniadis, and M. G. Kanatzidis, Science **303**, 818 (2004).
[33]G. S. Nolas, D. T. Morelli, and T. M. Tritt, Annu. Rev. Mater. Sci. **29**, 89 (1999).
[34]J. Capps, F. Drymiotis, S. Lindsey, and T. M. Tritt, Philos. Mag. Lett. **90**, 677 (2010).
[35]E. Chalfin, H. Lu, and R. Dieckmann, Solid State Ionics **178**, 447 (2007).
[36]G. J. Snyder, M. Christensen, E. Nishibori, T. Caillat, and B. B. Iversen, Nat. Mater. **3**, 458 (2004).
[37]H.-S. Kim, Z. M. Gibbs, Y. Tang, H. Wang, and G. J. Snyder, APL Mater. **3**, 041506 (2015).